DO LYα ABSORBERS CO-ROTATE WITH GALAXY DISKS?

David M. French, Bart P. Wakker
Department of Astronomy, University of Wisconsin, Madison, WI 53706, USA
Draft version March 6, 2018

ABSTRACT

We present results of a study comparing the relative velocity of Lyα absorbers to the rotation direction and velocity of nearby galaxy disks. We find...

Subject headings: galaxies:intergalactic medium, galaxies:evolution, galaxies:halos, quasars: absorption lines

1. INTRODUCTION

Our current ΛCDM cosmology picture describes galaxies forming hierarchically out of overdensities in the underlying dark matter distribution. As matter is funneled toward a growing galaxy, conservation of angular momentum redistributes the angular momentum in this gas to match that of the halo and underlying dark matter as the gas is shock-heated and slowly cools. As this infalling gas is responsible for birthing and continuing to feed the galaxies, it is expected that the extended gaseous halos should rotate in the same sense as both the galactic disks and dark matter halos. Galaxy rotation curves have been observed to extend at constant velocity out to... (cite...). It becomes increasingly difficult to measure gas rotation much farther from this however as the density rapidly decreases. Within this region the galaxy disks transition into circumgalactic medium (CGM), and eventually the CGM merges with the intergalactic medium (IGM). At what point, however, does the surrounding medium cease to circulate with the galaxy?

HYDRO? simulations such as those by Stewart et al. (2011, 2013) suggests that the bulk CGM kinematics out to (WHAT DISTANCE) may circulate, and that absorption in intervening QSO sightlines should be able to accurately capture this rotation signature. Observational confirmation, however, has be inconclusive. Côté et al. 2005 probed the halos of nine galaxies using *HST* observed background QSOs, finding large warps would be needed to explain the velocity of $H\,i$ absorbers by an extended rotating disk. Wakker & Savage (2009) compiled a sample of 4 galaxy-QSO systems from the literature, finding only 1/4 of Lyα absorbers appeared to co-rotate with the associated galaxy disk. Approaching the question from a different angle, Bowen et al. (2016) probed the halo of a single galaxy, NGC????, with 4 nearby QSO sightlines, and again found evidence for both co-rotation and

Numerous studies have shown a correlation between equivalent width and decreasing velocity difference between galaxies and IGM absorbers (e.g., French & Wakker 2017, MORE).

To make progress here, we have obtained rotation curves for 12 nearby spiral galaxies which are located within 500 kpc of a background QSO observed by Cosmic Origins Spectrograph (COS) on *HST*.

2. DATA AND ANALYSIS

2.1. *SALT Data*

Our sample contains 12 galaxies observed with the Southern African Large Telescope (SALT) Robert Stobie Spectrograph (RSS) in longslit mode. These 12 were selected from a larger pool of 48 submitted targets by the SALT observing queue. These 48 possible targets were chosen for their proximity to background QSOs whose spectra contained promising Lyα lines. Finally, we only included galaxies with $z \leq 0.33$ ($cz \leq 10,000$ km s^{-1}), angular sizes less than 6' to ensure easy sky subtraction, and surface brightnesses sufficient to keep exposure times below $\sim 1300s$. Table 2 summarizes these observations. Data was taken for 2 additional galaxies, NGC3640 and NGC2962, but proved unusable due to issues with spectral identification and low signal to noise (respectively).

All SALT galaxy spectra were reduced and extracted using the standard PySALT reduction package (**CITATION**), which includes procedures to prepare the data, correct for gain, cross-talk, bias, and overscan, and finally mosaic the images from different extensions. Next, we rectify the images with wavelength solutions found via Ne and Ar arc lamp spectra line identification. Finally, we perform a basic sky subtraction using an off-sky portion of the image, and extract 5-10 pixel wide 1-D strips from the reduced 2-D spectrum.

For each 1-D spectrum, we identify the Hα emission lines and perform a non-linear least-squares Voigt profile fit using the Python package LMFIT[1]. The line centroid and 1σ standard errors are returned, and these fits are then shifted to rest-velocity based on the galaxy systemic redshift and heliocentric velocity corrections are calculated with the IRAF rvcorrect procedure. The final rotation velocity is calculated by then applying the inclination correction, $v_{rot} = v/\sin(i)$. Final errors are calculated as

$$\sigma^2 = \left(\frac{\partial v_{rot}}{\partial \lambda_{obs}}\right)^2 (\Delta\lambda_{obs})^2 + \left(\frac{\partial v_{rot}}{\partial v_{sys}}\right)^2 (\Delta v_{sys})^2 + \left(\frac{\partial v_{rot}}{\partial i}\right)^2 (\Delta i)^2, \quad (1)$$

where $\Delta\lambda_{obs}$, Δv_{sys}, and Δi are the errors in observed line center, galaxy redshift, and inclination, respectively. We determine the inclination error by calculate the standard deviation of all axis ratio values available for each

---

[1] http://cars9.uchicago.edu/software/python/lmfit/contents.html

Target	Galaxy	R.A.	Dec.	z	Program	Grating	Obs ID	Obs Date	$T_{exp}*$ [ks]	S/N* [1238]
(1)	(2)	(3)	(4)	(5)	(6)	(7)	(8)	(9)	(10)	(11)
1H0419-577	NGC1566	04 26 00.7	-57 12 02.0	0.10400	11686	G130M	Obs ID	Obs Date	20429	75
1H0419-577	NGC1566	04 26 00.7	-57 12 02.0	0.10400	11686	G160M	Obs ID	Obs Date	15934	55
HE0429-5343	NGC1566	04 30 40.0	-53 36 56.0	0.04001	12275	G130M	Obs ID	Obs Date	2067	12
HE0435-5304	NGC1566	04 36 50.9	-52 58 47.0	0.42616	11520	G130M	Obs ID	Obs Date	8372	12
HE0435-5304	NGC1566	04 36 50.9	-52 58 47.0	0.42616	11520	G160M	Obs ID	Obs Date	8935	9
RBS567	NGC1566	04 39 38.7	-53 11 31.0	0.24300	11520	G130M	Obs ID	Obs Date	8176	17
RBS567	NGC1566	04 39 38.7	-53 11 31.0	0.24300	11520	G160M	Obs ID	Obs Date	8933	11
HE0439-5254	NGC1566	04 40 12.0	-52 48 18.0	1.05300	11520	G130M	Obs ID	Obs Date	8402	18
HE0439-5254	NGC1566	04 40 12.0	-52 48 18.0	1.05300	11520	G160M	Obs ID	Obs Date	8935	13
H1101-232	NGC3513	11 03 37.7	-23 29 31.0	0.18600	12025	G130M	Obs ID	Obs Date	13341	16
H1101-232	NGC3513	11 03 37.7	-23 29 31.0	0.18600	12025	G160M	Obs ID	Obs Date	13296	10
SDSSJ112005.00+041323.0	NGC3633	11 20 05.0	+04 13 23.0	0.54689	12603	G130M	Obs ID	Obs Date	4708	9
RX_J1121.2+0326	CGCG039-137	11 21 14.0	+03 25 47.0	0.15200	12248	G130M	Obs ID	Obs Date	2695	5
RX_J1121.2+0326	NGC3633	11 21 14.0	+03 25 47.0	0.15200	12248	G130M	Obs ID	Obs Date	2695	5
RX_J1121.2+0326	CGCG039-137	11 21 14.0	+03 25 47.0	0.15200	12248	G160M	Obs ID	Obs Date	4741	4
RX_J1121.2+0326	NGC3633	11 21 14.0	+03 25 47.0	0.15200	12248	G160M	Obs ID	Obs Date	4741	4
SDSSJ112224.10+031802.0	CGCG039-137	11 22 24.1	+03 18 02.0	0.47528	12603	G130M	Obs ID	Obs Date	7588	10
3C273.0	NGC4536	12 29 06.7	+02 03 09.0	0.15834	12038	G130M	Obs ID	Obs Date	4002	111
3C273.0	NGC4536	12 29 06.7	+02 03 09.0	0.15834	1140	G160M	Obs ID	Obs Date	30028	55
HE1228+0131	NGC4536	12 30 50.0	+01 15 23.0	0.11700	11686	G130M	Obs ID	Obs Date	11036	61
HE1228+0131	NGC4536	12 30 50.0	+01 15 23.0	0.11700	11686	G160M	Obs ID	Obs Date	11029	45
LBQS1230-0015	NGC4536	12 33 04.1	-00 31 34.0	0.47095	11598	G130M	Obs ID	Obs Date	10323	13
LBQS1230-0015	NGC4536	12 33 04.1	-00 31 34.0	0.47095	11598	G160M	Obs ID	Obs Date	5896	7
PG1302-102	NGC4939	13 05 33.0	-10 33 19.0	0.27840	12038	G130M	Obs ID	Obs Date	5979	27
PG1302-102	NGC4939	13 05 33.0	-10 33 19.0	0.27840	12038	G160M	Obs ID	Obs Date	6867	34
SDSSJ135726.27+043541.4	NGC5364	13 57 26.3	+04 35 41.0	1.23453	12264	G130M	Obs ID	Obs Date	14148	15
SDSSJ135726.27+043541.4	NGC5364	13 57 26.3	+04 35 41.0	1.23453	12264	G160M	Obs ID	Obs Date	28206	12
QSO1500-4140	NGC5786	15 03 34.0	-41 52 23.0	0.33500	11659	G130M	Obs ID	Obs Date	9258	9
SDSSJ151237.15+012846.0	UGC09760	15 12 37.2	+01 28 46.0	0.26625	12603	G130M	Obs ID	Obs Date	7590	6
RBS1768	ESO343-G014	21 38 49.9	-38 28 40.0	0.18299	12936	G130M	Obs ID	Obs Date	6962	24
RBS1768	ESO343-G014	21 38 49.9	-38 28 40.0	0.18299	12936	G160M	Obs ID	Obs Date	3837	11
MRC2251-178	MCG-03-58-009	22 54 05.9	-17 34 55.0	0.06609	12029	G130M	Obs ID	Obs Date	5515	42
MRC2251-178	MCG-03-58-009	22 54 05.9	-17 34 55.0	0.06609	12029	G160M	Obs ID	Obs Date	7125	30
RBS2000	IC5325	23 24 44.7	-40 40 49.0	0.17359	13448	G130M	Obs ID	Obs Date	5046	18
RBS2000	IC5325	23 24 44.7	-40 40 49.0	0.17359	13448	G160M	Obs ID	Obs Date	5726	12

Table 1
COS targets in this sample. *Total exposure time and S/N ratio is given for multi-orbit exposures.

galaxy in NED. The final physical scale is calculated using the SALT image scale of 0.1267 arcsec/pixel, multiplied by the 4-pixel spatial binning, and converted to physical units using a redshift-independent distance if available, and a Hubble flow estimate if not. We adopt a Hubble constant of $H_0 = 71$ km s^{-1}Mpc^{-1} throughout.

Finally, we calculate our approaching and receding velocities via a weighted mean of the outer $1/2$ of each rotation curve, with errors calculated as weighted standard errors in the mean. Our final redshifts are calculated by forcing symmetric rotation, such that the outer $1/2$ average velocity for each side matches. See Figure **??** for an example.

2.2. *COS Spectra*

The Barbara A. Mikulski Archive for Space Telescopes (MAST) archives yield 19 QSO targets observed by COS which lie within 500 kpc of our SALT galaxies. These targets vary widely in signal-to-noise from approximately 5 to 100 due to our choosing them based only on their proximity to galaxies with known rotation. The reduction procedure for these spectra follow those described

by French & Wakker 2017 and Wakker et al. (2015). In short, spectra are processed with CALCOS vXXXX? and combined via the method of Wakker et al. (2015), which helps corrects the COS wavelength scale misalignments produced by CALCOS. Multiple exposures are combined via alignment with Galactic 21cm absorption spectra and summing total counts per pixel before converting to flux. The COS instrument is described in detail by Green et al. (2012).

3. SALT GALAXIES

3.1. *CGCG039-137*

CGCG039-137 is an isolated Scd type galaxy with a measured systemic velocity of 6918 ± 24 km s^{-1} and inclination of $63°$. There are two associated sightlines: RX_J1121.2+0326 at an impact parameter of 99 kpc and azimuth angle of $71°$ on the receding side, and SDSSJ112224.10+031802.0 at 491 kpc and $24°$ on the approaching side. Lyα absorption is detected in both sightlines within 400km s^{-1} of CGCG039-137.

Towards RX_J1121.2+0326 we detect Lyα at 6975 km s^{-1} , which, at $\Delta v = 57$ km s^{-1}, lies well

.

Galaxy	R.A.	Dec.	cz (km s^{-1})	Type	Grating	V$_{rot}$ [km s^{-1}]	V$_{rot}$/sin(i) [km s^{-1}]	Obs Date	T_{exp} [ks]
(1)	(2)	(3)	(4)	(5)	(6)	(7)	(8)	(9)	(10)
CGCG039-137	11 21 26.95	+03 26 41.68	6918 ± 24	Scd	PG2300	132 ± 16	139 ± 26	05 11 2016	700
IC5325	23 28 43.43	−41 20 0.49	1512 ± 8	SAB(rs)bc	PG2300	53 ± 5	125 ± 39	05 17 2016	600
MCG-03-58-009	22 53 40.85	−17 28 44.00	9015 ± 19	Sc	PG2300	150 ± 12	171 ± 23	05 16 2016	1200
NGC1566	04 20 0.42	−54 56 16.12	1502 ± 15	SAB(rs)bc	PG2300	64 ± 8	195 ± 47	10 18 2016	400
NGC3513	11 03 46.08	−23 14 43.8	1204 ± 12	SB(s)c	PG2300	11 ± 10	22 ± 24	05 26 2016	600
NGC3633	11 20 26.22	+03 35 8.20	2587 ± 7	SAa	PG2300	149 ± 6	157 ± 9	05 11 2016	1200
NGC4536	12 34 27.05	+02 11 17.30	1867 ± 33	SAB(rc)bc	PG2300	129 ± 9	148 ± 41	05 11 2016	1300
NGC4939	13 04 14.39	−10 20 22.60	3093 ± 33	SA(s)bc	PG2300	204 ± 25	275 ± 66	05 14 2016	500
NGC5364	13 56 12.00	+05 00 52.09	1238 ± 17	SA(rs)bc pec	PG2300	130 ± 13	155 ± 22	05 11 2016	700
NGC5786	14 58 56.26	−42 00 48.10	2975 ± 22	SAB(s)bc	PG2300	156 ± 10	172 ± 25	05 11 2016	250
RFGC3781	21 37 45.18	−38 29 33.22	9139 ± 32	S	PG2300	203 ± 32	203 ± 32	05 16 2016	1000
UGC09760	15 12 02.44	+01 41 55.46	2094 ± 16	Sd	PG2300	46 ± 10	46 ± 16	05 11 2016	500

Table 2
SALT targeted galaxies. Columns are as follows: 1) the galaxy name, 2), 3) R.A., Dec. in J2000, 4) galaxy systemic velocity, 5) morphological type (RC3), 6) RSS grating used, 7) approaching side velocity, 8) receding side velocity, 9) observation date, 10) exposure time, and 11) S/N of the Hα or Ca H&K lines.

within the range of projected velocities consistent with co-rotation. The absorber detected toward SDSSJ112224.10+031802.0 occurs at a more distant 6606 km s^{-1}($\Delta v = -312$ km s^{-1}). Although this absorber has the correct sign for co-rotation (blue-ward on the approaching side of the disk), the large velocity difference and impact parameter make it unlikely that this absorption can be linked to coherent halo rotation.

3.2. *ESO343-G014*

ESO343-G014 is an edge on spiral galaxy with a measured systemic velocity of 9138.9 ± 31.7 km s^{-1}. It has a smaller neighboring galaxy, 2MASXJ21372816-3824412, located north of it's major axis at a projected distance of 216 kpc and velocity of 9129. The nearest sightline is towards RBS1768 at an impact parameter of 466kpc and 74° azimuth angle on the approaching side. We detect 3 Lyα absorption lines within 300 km s^{-1}of ESO343-G014 (at 9308, 9360, and 9434 km s^{-1}). All of these are anti-aligned with the rotation of ESO343-G014, but unfortunately the presence of 2MASXJ21372816-3824412 makes it difficult to attribute this gas solely to ESO343-G014. Additionally, this gas could be attributed to either the approaching or receding side of the disk due to the large impact parameter and high azimuth angle of the sightline.

3.3. *IC5325*

IC5325 is a face-on SAB(rs)bc type galaxy with a measured velocity of 1511.9 ± 8.4 km s^{-1}. It's inclination is just high enough (25°) to obtain a reasonable rotation curve. The closest neighboring galaxy is ESO347-G020 to the Southeast at 306 kpc and a heliocentric velocity of 1745 km s^{-1}. Three other much smaller galaxies are also located ~ 450 kpc to the Southwest. We detect Lyα absorption at 1598km s^{-1}, $\Delta v = 86$km s^{-1} in the spectrum towards RBS2000 at an impact parameter of 314 kpc and azimuth angle of 64° on the approaching side. While this velocity is anti-aligned with the rotation the disk gas, the low inclination angle of IC5325 leads to a highly uncertain position angle. Without additional observations, we cannot say for certain if the location of RBS2000 actually lies on the approaching or receding side. This position angle uncertainty also means our SALT rotation curve is a lower limit on the true rotation velocity of IC5325.

3.4. *MCG-03-58-009*

MCG-03-58-009 is a massive and very isolated Sc type galaxy at a measured velocity of 9015 ± 19 km s^{-1} and inclination angle of 49°. A weak Lyα absorber is detected at 9029 km s^{-1} towards MRC2251-178, which lies 355 kpc away at an azimuth angle of 71° on the receding side. Although this absorber matches the velocity direction expected for co-rotation, the velocity difference ($\Delta v = 14$ km s^{-1}) is within the systemic velocity uncertainty. The relative weakness of this absorber (EW = 62 ± 4 mÅ) is somewhat surprising given it's proximity (just outside of 1 R_{vir}) to a massive galaxy. If this is representative of an isolated system such as MCG-03-58-009, then we should expect the halo rotational velocity to approach systemic by 1 R_{vir}.

3.5. *NGC1566*

NGC1566 is well sampled (5 nearby QSO sightlines), but unfortunately also part of a complex environment of neighboring galaxies. We detect Lyα in all 5 of these sightlines. The farthest three, HE0439-5254, RBS567, and HE0435-5304, are clustered close together to the northeast of NGC1566 at $\gtrsim 395$ kpc and azimuth angles of $\sim 60°$.

HE0429-5343 is in the same direction and azimuth angle but closer at $\rho = 256$ kpc, and shows Lyα absorption at 1167 and 1358 km s^{-1}. These absorbers both have the correct velocity *sign*, but we would expect a smaller velocity for co-rotation (approximately $\Delta v \sim \pm 40$ km s^{-1} projected). This difference could be explained by invoking either a warped extended disk, or perhaps inflowing gas.

1H0419-577 is located to the south at 303 kpc and just east of the receding side of the major axis at an azimuth angle of 10°. We detect Lyα at 1071, 1123, 1188, 1264, and 2020 km s^{-1}, all of which are the wrong sign for co-rotation or distant in velocity. This sightline is actually closer to a small group of galaxies including
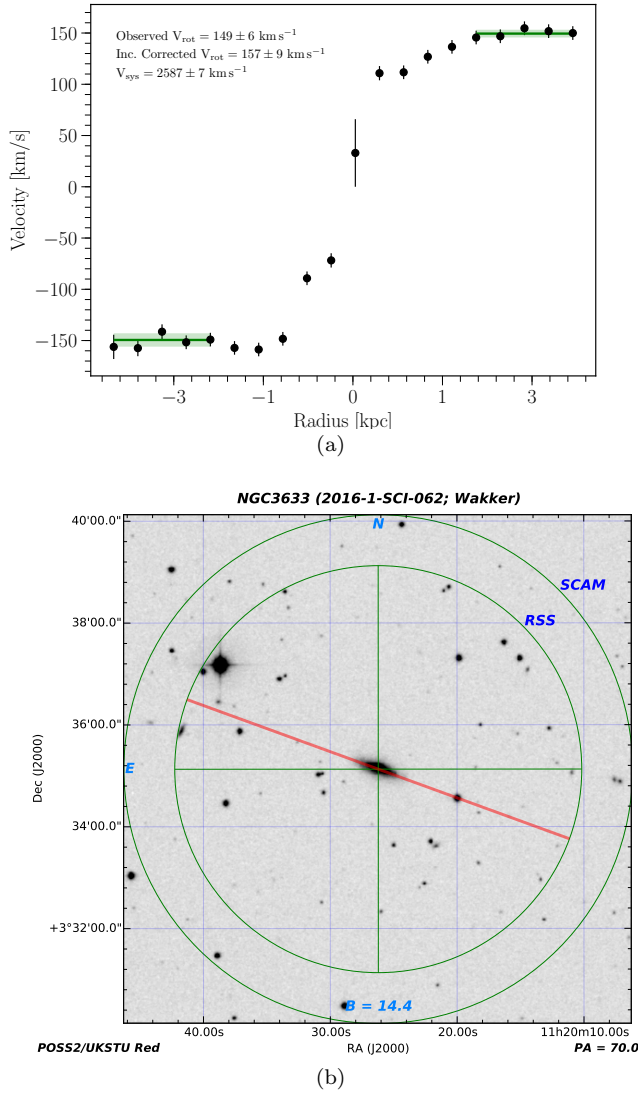
(a)

NGC3633 (2016-1-SCI-062; Wakker)

POSS2/UKSTU Red   PA = 70.0

(b)

Figure 1. a) Rotation curve of NGC3633. The solid green line indicates the weighted mean velocity over the corresponding x-axis region, and the shaded green indicates the 1σ error in the mean. b) SALT finder chart for NGC3633 showing the position of the slit in red.

NGC1549, NGC1546 and NGC1536, all with systemic velocities near 1200 $\mathrm{km\,s^{-1}}$. We expect the lines at 1071, 1123, 1188, 1264 $\mathrm{km\,s^{-1}}$ to be associated with this group rather than with NGC1566.

3.6. *NGC3513*

NGC3513 a mostly face-on SB(rs)c galaxy with heliocentric velocity $V_{hel} = 1204 \pm 12$ $\mathrm{km\,s^{-1}}$. It has a companion galaxy in NGC3511 at an impact parameter of 44 kpc at $v_{hel} = 1109$ $\mathrm{km\,s^{-1}}$. We detect Lyα at 1182 $\mathrm{km\,s^{-1}}$ toward background QSO H1101-232, which is located directly south at 60 kpc and azimuth angle of 67° on the receding side. NGC3513 appears to be rotating slowly, with a maximal inclination-corrected rotation velocity of 22 ± 24 $\mathrm{km\,s^{-1}}$. The $\Delta v = -22$ $\mathrm{km\,s^{-1}}$ for this absorber matches well with the magnitude of this rota-

tion, but is opposite in sign for co-rotation. Given that NGC3511 is so close, this absorber's velocity is probably subject to a complex velocity field influenced by both NGC3511 and NGC3513.

3.7. *NGC3633*

Several locations show two velocities for emission. We have combined these into a single velocity measurement via a weighted average. We measure a redshift for this galaxy of $cz = 2597.6 \pm 2.4$ $\mathrm{km\,s^{-1}}$.

We measure a line-of-sight rotation velocity for NGC3633 of $v_{rot} = 139 \pm 3.3,\ -160 \pm 5.7,\ \mathrm{km\,s^{-1}}$.

Systemic velocity as published: 2600 Velocity as measured: 2587.2 ± 6.6 Rotation velocity (inc corrected) 157 ± 11 $\mathrm{km\,s^{-1}}$ Rotation velocity (observed) 149 ± 6 $\mathrm{km\,s^{-1}}$ Inclination: 69 Adjusted Inc: 72 Morphology: SAa $L_* = 0.88$

Three sightlines:
SDSSJ112005.00+041323.0 at 468 kpc, 78deg az:
2285 Lya (dv = -302 $\mathrm{km\,s^{-1}}$ on neg side) 2578 Lya (dv = -9 $\mathrm{km\,s^{-1}}$ on neg side)
RX_J1121.2+0326 at 184 kpc, 58deg az:
2605 Lya (dv = 18 $\mathrm{km\,s^{-1}}$ on neg side)
SDSSJ112224.10+031802.0 at 413 kpc, 50deg az:
Nothing

3.8. *NGC4536*

The data on the receding side of NGC4536 is very messy, and may include contamination from background sources.

Systemic velocity as published: 1808 Velocity as measured: 1866.9 ± 32.9 Rotation velocity (inc corrected) 139 ± 37 $\mathrm{km\,s^{-1}}$ Rotation velocity (observed) 129 ± 32 $\mathrm{km\,s^{-1}}$ Inclination: 59 Adjusted Inc: 61 Morphology: SAB(rs)bc $L_* = 2.0$

Three sightlines:
3C273.0 at 349 kpc, 11deg az:
1580 Lya (dv = -287 $\mathrm{km\,s^{-1}}$ on pos side) 2156 Lya (dv = 289 $\mathrm{km\,s^{-1}}$ on pos side) 2267 Lya (dv = 400 $\mathrm{km\,s^{-1}}$ on pos side)
HE1228+0131 at 338 kpc, 51deg az:
1495 Lya (dv = -372 $\mathrm{km\,s^{-1}}$ on pos side) 1571 Lya (dv = -296 $\mathrm{km\,s^{-1}}$ on pos side) 1686 Lya (dv = -181 $\mathrm{km\,s^{-1}}$ on pos side) 1721 Lya (dv = -146 $\mathrm{km\,s^{-1}}$ on pos side) 1854 Lya (dv = -13 $\mathrm{km\,s^{-1}}$ on pos side) 2311 Lya (dv = 444 $\mathrm{km\,s^{-1}}$ on pos side)
SDSSJ123748.99+012607.0 at 294 kpc, 37deg az:
not finished

3.9. *NGC4939*

Systemic velocity as published: 3110 Velocity as measured: 3092.8 ± 33 Rotation velocity (inc corrected) 275 ± 49 $\mathrm{km\,s^{-1}}$ Rotation velocity (observed) 204 ± 25 $\mathrm{km\,s^{-1}}$ Inclination: 46 Adjusted Inc: 48 Morphology: SA(s)bc $L_* = 5.5$

One sightline:
PG1302-102 at 254 kpc, 61deg az:
3448 Lya (dv = 355 $\mathrm{km\,s^{-1}}$ on neg side)

3.10. *NGC5364*

Systemic velocity as published: 1241 Velocity as measured: 1238.0 ± 16.9 Rotation velocity (inc corrected) 155 ± 27 km s^{-1}Rotation velocity (observed) 130 ± 13 km s^{-1}Inclination: 55 Adjusted Inc: 57 Morphology: SA(rs)bc $L_* = 1.9$

Two sightline:
SDSSJ135309.50+033328.0 at 519 kpc, 21deg az:
not finished
SDSSJ135726.27+043541.4 at 165 kpc, 84deg az:
1124 Lya (dv = -114 km s^{-1}on pos? side) 1296 Lya (dv = 58 km s^{-1}on pos? side)

3.11. *NGC5786*

Systemic velocity as published: 2998 Velocity as measured: 2974.6 ± 21.5 Rotation velocity (inc corrected) 172 ± 28 km s^{-1}Rotation velocity (observed) 156 ± 19 km s^{-1}Inclination: 63 Adjusted Inc: 65 Morphology: (R'_2)SAB(s)bc $L_* = 25$

One sightline:
QSO1500-4140 at 453 kpc, 1deg az:
3141 Lya (dv = 166 km s^{-1}on pos side)

3.12. *UGC09760*

Systemic velocity as published: 2023 Velocity as measured: 2093.7 ± 15.5 Rotation velocity (inc corrected) 46 ± 16 km s^{-1}Rotation velocity (observed) 46 ± 12 km s^{-1}Inclination: 85 Adjusted Inc: 90 Morphology: Sd $L_* = 0.17$

Two sightlines:
SDSSJ151237.15+012846.0 at 123 kpc, 90deg az:
2051 Lya (dv = -43 km s^{-1}on minor axis. Looks neg side, but extremely close)

3.13. *Ancillary Data*

To increase our sample size we have also searched the literature for galaxies with published rotation curves and orientations. Unfortunately, while the rotation velocity is available for thousands of galaxies, only a handful also include the *orientation* of the rotation on the sky.

4. HALO ROTATION MODEL

In order to better understand how QSO sightlines probe intervening velocity structure we have developed a simple halo gas rotation model. This model is seeded by an observed rotation curve (or whatever rotation curve-esque data suits ones fancy). This input curve is then interpolated and extended out to $2R_{vir}$ based on the average velocity of the outer 1/2 radius. Next, we project this interpolated rotation curve onto a plane oriented to a faux QSO sightline identically to the input galaxy-QSO pair orientation. By stacking multiple rotation-planes in the galaxy z-axis direction, we then create a simple cylindrical rotating halo model. Finally, each rotation-plane in the stack is projected onto the faux sightline. The result is a function representing the rotation velocity encountered by the sightline as a function of velocity (or distance) along it.

For each galaxy-QSO pair we created 3 rotation models: 1) a purely cylindrical halo extending $1R_{vir}$ in height and $2R_{vir}$ in radius, 2) a spherical halo extending $2R_{vir}$ in radius, and 3) a cylindrical model extending $1R_{vir}$ in height and $2R_{vir}$ in radius with rotation velocities which smoothly decline to systemic towards these boundaries.

5. DISCUSSION
6. SUMMARY

- First result

Facilities: HST (COS)

Figure 2. A map of the locations of each absorber normalized with respect to the galaxy virial radius. Concentric rings indicate distances of 1, 2 and 3 R_{vir}. All galaxies are rotated to PA = 90, such that their major axis' are horizontal. The color of the points indicates their line-of-sight velocity compared to that of the rotation of the nearby galaxy. Blue indicates co-rotation, red indicates anti-rotation, and yellow indicates cases where either is possible due to a combination of orientation and velocity uncertainties. The size of each point is scaled to reflect the EW of the absorber.